JOURNAL OF MATERIALS SCIENCE 23 (1988) 1106–1111

Influence of thickness on H_2 gas sensor properties in polycrystalline SnO_x films prepared by ion-beam sputtering

TAKEYUKI SUZUKI, TSUTOMU YAMAZAKI, HIROSHI YOSHIOKA, KUNIYUKI HIKICHI
Department of Industrial Chemistry, Faculty of Technology, Tokyo University of Agriculture and Technology, Koganei, Tokyo 184, Japan

Amorphous SnO_x films were deposited on sintered alumina substrates by ion-beam sputtering. They were annealed at 500° C for 2 h in air and polycrystalline films with thickness varying from about 1 to 700 nm were prepared. Film-sensor properties against 0.47% H_2 gas were measured as a function of thickness and the operating temperature for 150 to 350° C. The film thickness exhibiting a sensitivity maximum increased gradually with temperature. The optimum thickness shifted from 7 nm at 150° C to 175 nm at 350° C. Highly sensitive films lay in a narrow thickness range of 60 to 180 nm and films thinner or thicker than this were relatively insensitive at 300 and 350° C. A model was proposed to interpret the sensitivity behaviour in terms of thickness and grain-boundary effect.

1. Introduction

The gas sensitivities of films of doped- or undoped-tin oxide depend highly on the deposition techniques and the post-annealing. The influence of thickness on sensor properties has been reported on films prepared by sputtering [1–3], spraying [4, 5] and chemical vapour deposition (CVD) method [6]. During the study of gas sensor properties in ion-beam sputtered SnO_x, amorphous films showed a strong thickness dependence of sensitivity and resistivity [7, 8]. They exhibited a high sensitivity at a thickness between 5 and 20 nm and a resistivity maximum at about 7 nm. The sensitivity of films thinner than 5 nm and thicker than 50 nm was negligibly small. This unexpected thickness dependence of amorphous SnO_x films led to the further film-sensor investigation in polycrystalline SnO_x films reported here.

2. Experimental methods

The relationship between film thickness (sputtering time), sensitivity, resistivity and operating temperature was examined on films annealed at 500° C for 2 h in air. Details of film deposition, X-ray diffraction and measurement of electrical resistance were the same as described previously [7, 9]. The gas sensitivity was defined as the ratio of the resistance in synthetic air (s-air) to that in 0.47% H_2. Most films were deposited on sintered alumina substrates (Furuuchi Chemicals, Japan). These substrates have a theoretical density of $>96\%$ and the surface roughness is 4 μm. Unless otherwise specified, films were deposited on sintered alumina substrates. Four other substrates, such as optical-flat fused silica and pyrex glasses, mullite and magnesia plates, were also used to examine the substrate effect on sensor properties. Mullite and magnesia plates were cut from the sintered tubes and served as substrates as-prepared with a very rough surface. The mullite plate has a theoretical density of 100%. The magnesia plate has an apparent porosity of about 20%.

3. Results and discussion

3.1. Film structure

The film thickness deposited after 2 h was 350 nm. The thickness of other films was calculated using this rate. X-ray diffraction diagrams of as-deposited and annealed films are shown in Fig. 1. As-deposited films were amorphous with a trace amount of the trigonal Sn_3O_4 (JCPDS 20-1293). Sensor properties of these films have been reported previously [7, 8] and are cited here as that of amorphous films. Films annealed at 500° C for 2 h in air were polycrystalline tetragonal SnO_2 (JCPDS 21-1250) with a trace amount of the trigonal Sn_3O_4; grains were randomly oriented.

3.2. Response curve

Typical examples of the response curve are given in Fig. 2. These films were deposited for 30 min. A small peak in Fig. 2a on the first introduction of s-air arises from the desorption of H_2O contained in ordinary air. Generally, output voltage, V, increased with the introduction of 0.47% H_2 and decreased in contact with s-air. This increase and decrease in V corresponded to desorption and adsorption of oxygen, respectively. The desorption rate is slow and the adsorption rate is rather fast. Sensitivity and 90% response time of the film sensor shown in Fig. 2a were 14 and 270 sec and those in Fig. 2b were 258 and 2430 sec. The latter sensitivity was the highest, and the response time was the longest of all films examined.

0022–2461/88 $03.00 + .12

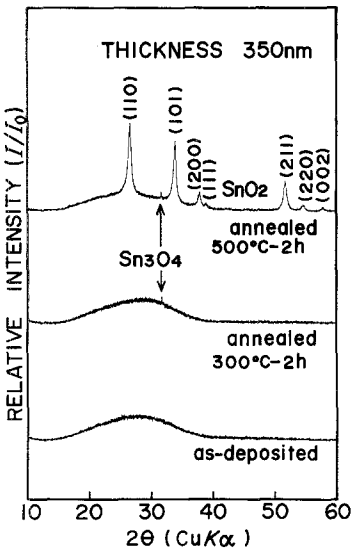

Figure 1 X-ray diffraction diagram.

3.3. Sensitivity

Figs. 3 to 6 show sensitivity as a function of sputtering time at 150, 250, 300 and 350° C, respectively. The thickness dependence of sensitivity at 150° C (Fig. 3) is similar to that of amorphous films [7]. The high sensitivity region is limited to a narrow thickness range from 4 (72 sec) to 9 nm (180 sec). Other films are almost insensitive against H_2 gas. At 250° C (Fig. 4), the sensitivity of films thicker than 9 nm (180 sec) increased to nearly twice of that at 150° C. However, films thinner than 2 nm (38 sec) and thicker than 525 nm (10 800 sec) remained insensitive. The general trend at 250° C is similar to that at 150° C. At 300° C (Fig. 5), the sensitivity of thicker films continued to increase except for the two thickest films. Further increase in operating temperature up to 350° C (Fig. 6) accelerated these tendencies. Here the sensitivity of films between 4 (72 sec) and 13 nm (270 sec) decreased, while films ranging from 17 (360 sec) to 350 nm (7200 sec) continued to increase.

The thinnest three films and the thickest two films, however, always remained insensitive. The thickness effect on the temperature dependence of sensitivity is clearly demonstrated when the sensitivity at 150° C (Fig. 3) is compared with that at 350° C (Fig. 6). A model was constructed to interpret qualitatively this

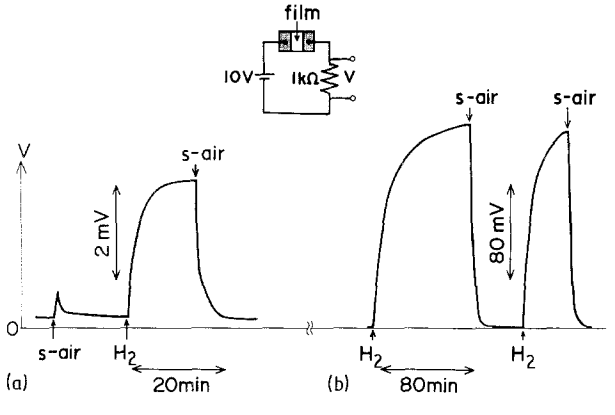

Figure 2 Response characteristics of film-sensors. (a) Thickness 87 nm, $d = 455\,\mu m$, 350° C. (b) Thickness 87 nm, $d = 80\,\mu m$, 300° C.

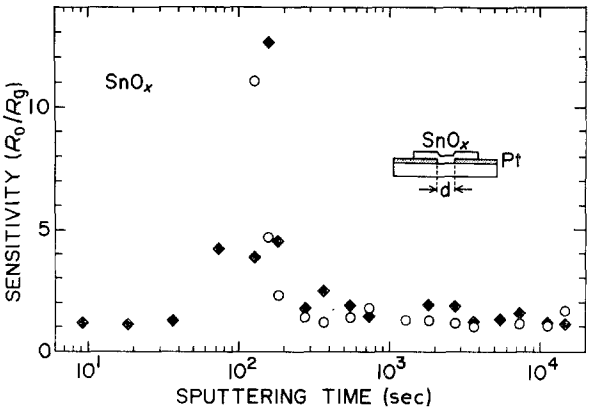

Figure 3 Sensitivity at 150° C as a function of sputtering time. Deposition rate 0.049 nm sec^{-1}, (○) $d = 455 \pm 5\,\mu m$, (◆) $d = 80 \pm 20\,\mu m$.

different sensitivity behaviour. The model shown in Fig. 7 represents the film thickness, operating temperature and the depletion region due to adsorbed oxygen in s-air. We have made the model with the following assumptions: (1) grain size is the same order of magnitude as the film thickness; (2) oxygen is adsorbed on the film surface and no preferred adsorption on grain boundaries occurs at 150° C; (3) surface electrons bound to adsorbed oxygen form a flat depletion layer, the thickness of which is around 8 nm at 150° C; (4) preferred adsorption on grain boundaries is dominant at 350° C. At this temperature, adsorption on other parts of the surface also increases when the film is thick enough; (5) the depletion depth of about 180 nm is formed by negatively charged oxygen at the boundaries at 350° C, (6) the deepest depletion becomes equal to the film thickness in films thinner than 180 nm at 350° C. This arises from the reduction of negatively charged oxygens at the boundaries to maintain the electrical neutrality condition between donors and electrons. Assumption 6 is further depicted schematically in Fig. 8. Adsorption of oxygen on a unit length of grain boundary being the same, the deepest depletion region occurs just beneath the points where the surface grain boundary meets. Although the deepest depletion hinders the movement of free electrons, they can flow freely from grain to grain through an interconnected conduction channel. Let us now consider what this model predicts. When hydrogen is introduced it reacts with adsorbed oxygen

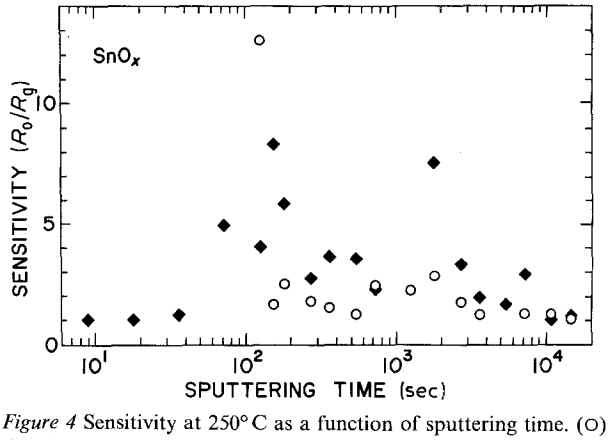

Figure 4 Sensitivity at 250° C as a function of sputtering time. (○) $d = 455\,\mu m$, (◆) $d = 80\,\mu m$.

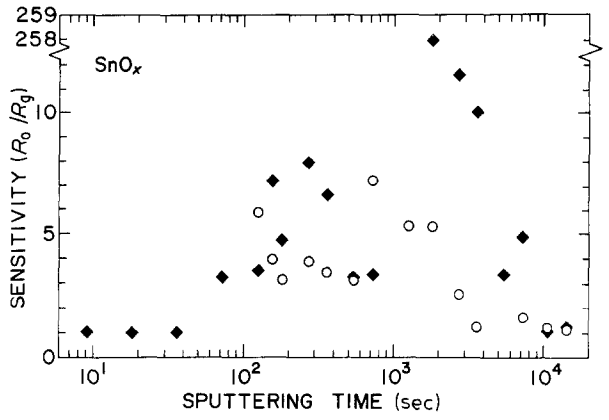

Figure 5 Sensitivity at 300° C as a function of sputtering time. (○) $d = 455\,\mu m$, (◆) $d = 80\,\mu m$.

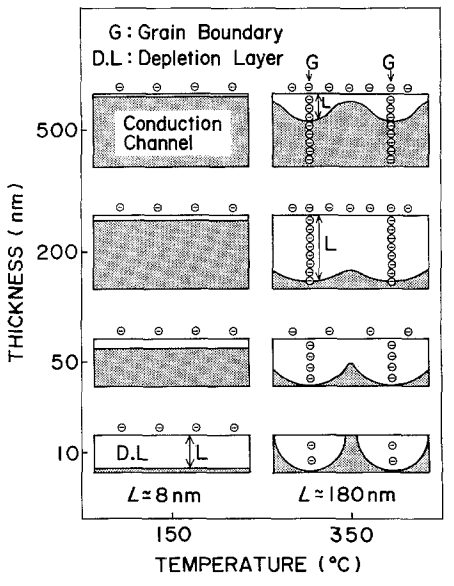

Figure 7 A model illustrating the effect of film thickness on the depletion region in s-air.

to form H_2O molecules [10]. This results in reduction of adsorbed oxygen and, consequently, the surface electrons are ejected into the film as conduction electrons. Thus the depletion region is reduced and the conduction channel is widened by the introduction of hydrogen. As the resistance of the film is supposed to be inversely proportional to the area of the conduction channel, the gas sensitivity is approximated by the (area ratio of conduction channel)$^{-1}$ defined as (total area of the cross-section)/(area of the conduction channel). Thus the proposed model can explain the following experimental facts: (1) the sensitivity maximum occurs at about 8 nm (160 sec) at 150° C and at about 180 nm (3700 sec) at 350° C; (2) high sensitivity is maintained for films thinner than 180 nm at 350° C, however the sensitivity decreases gradually as the film becomes thinner; (3) films with a small area ratio of depletion layer exhibit a low sensitivity. This corresponds to films thicker than 50 nm (1000 sec) at 150° C and to films thicker than 500 nm (1000 sec) at 350° C.

The model further indicates that a film sensor with a more uniform and a smaller grain size exhibits a better performance. These factors contribute to make the depletion region more flat and deeper thus leading a film to a high sensitivity. So far we have described the sensitivity of films thicker than about 10 nm (200 sec). The sensitivity or conduction mechanism of films thinner than 10 nm seems different from the proposed model. This is mentioned in the next section, but first let us look at the response time. Fig. 9 shows the response time as a function of sputtering time for films with sensitivity higher than four. These response times should be regarded as only tentative, because the inlet gas was not necessarily aimed directly at the film sensor. Nevertheless we see a tendency for the response time to increase gradually as the thickness increases from about 9 nm (180 sec) to 350 nm (7200 sec). The thinnest film, 4 nm (72 sec), exhibited a rather longer response time compared to other films around 10 nm (200 sec).

3.4. Resistivity

Figs. 10 and 11 show resistivity in s-air as a function of sputtering time for films with different electrode gaps together with the resistivity of amorphous films at 150° C [7]. The resistance of films thinner than 5 nm (100 sec) with a larger electrode gap was too high to be measured. Two outstanding features were observed in films with a smaller electrode gap (Fig. 10). One is the decrease in resistivity as the film becomes thinner than 4 nm (72 sec). The other is the hole conduction observed in some films between 4 (72 sec) and 7 nm (153 sec). The latter evidence was obtained from the measurement of the sign of the Seebeck coefficient. Ultrathin films less than about 10 nm (200 sec) probably

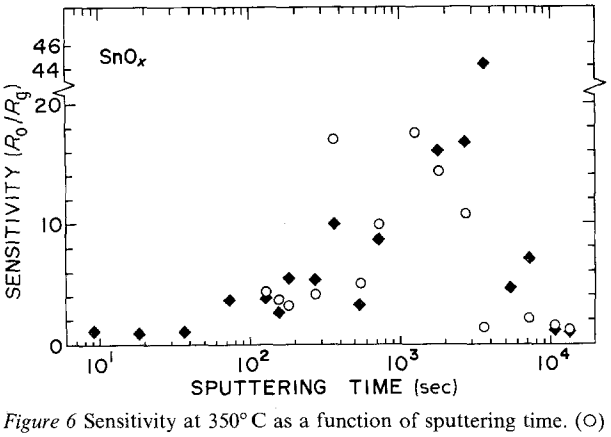

Figure 6 Sensitivity at 350° C as a function of sputtering time. (○) $d = 455\,\mu m$, (◆) $d = 80\,\mu m$.

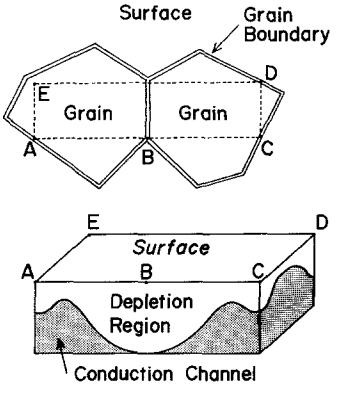

Figure 8 Surface grain boundary and the induced depletion region due to negatively adsorbed oxygen at the boundary.

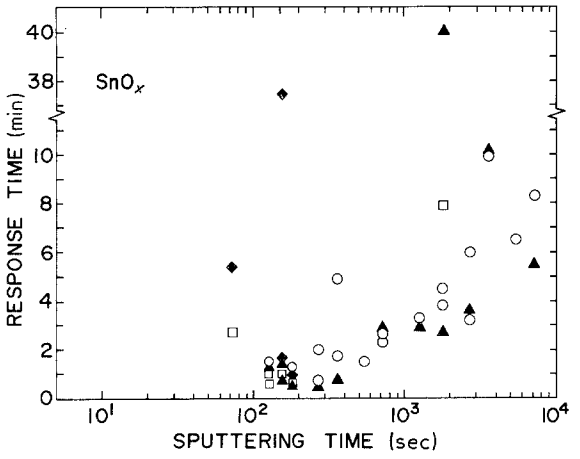

Figure 9 90% response time of films with sensitivity higher than 4, as a function of sputtering time. (○) 350° C, (▲) 300° C, (□) 250° C, (◆) 150° C.

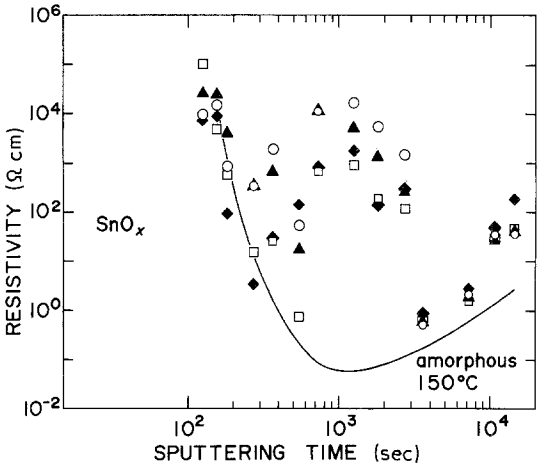

Figure 11 Resistivity of films with the electrode gap of 455 ± 5 μm in s-air. d = 455 μm. (○) 350° C, (▲) 300° C, (□) 250° C, (◆) 150° C.

behave differently from a normal n-type semiconductor. This is the reason why the present model treats only films thicker than about 10 nm (200 sec). Detailed investigation for these anomalies is now underway.

A survey of Figs 10 and 11 shows that the electrode gap is also a factor for controlling the resistivity. Although similar behaviour has been observed in amorphous films, the cause of this gap dependency is not clear. Turning back to the model (Fig. 7), let us now examine what it predicts qualitatively on the resistivity in s-air. It is well known that the resistivity becomes independent of the thickness for thick films of the order of 100 to 1000 nm or more [1, 5, 6]. Here we pick up only two factors, grain boundary and depletion region, to estimate the effect of thickness on resistivity. Naturally our estimation which follows cannot be extended to thicker films with a constant resistivity. According to assumption 1, the grain-boundary density, and therefore the grain-boundary resistance, increases as the thickness decreases. Thus we presume that the resistivity of a film is inversely proportional to the thickness. Another factor is the area of the conduction channel. As already described, resistivity is inversely proportional to the area ratio of the conduction channel. Therefore we assume that the total resistivity of a film is approximately proportional to (film thickness)$^{-1}$ × (area ratio of the conduction channel)$^{-1}$. For the resistivity at 150° C, both factors increase as the film thickness decreases. Thus the resistivity is supposed to increase monotonically with the decrease of the thickness. On the other hand, the boundary effect induces a sensitivity maximum at 350° C at a thickness where the (area ratio of the conduction channel)$^{-1}$ is the largest. The factor (thickness)$^{-1}$ makes the peak broaden and shifts the maximum towards a thinner thickness side. Thus the model predicts that a broad resistivity maximum occurs at 350° C at a thickness thinner than that of the sensitivity maximum. In fact, a resistivity maximum is clearly observed at 61 nm (1260 sec) for the film with a larger electrode gap (Fig. 11) at 350° C. However, monotonical increase in resistivity down to 10 nm (200 sec) at 150° C could not be observed, firstly because the measured values scattered in thinner films, and secondly because the resistivity depended on the electrode gap. The scatter is probably due to an incorporation of impurities and also to irregular grain size distribution grown on sintered alumina substrates with uneven surfaces.

It is to be noted that an amorphous film is an ideal material for a model where the effect of a flat depletion

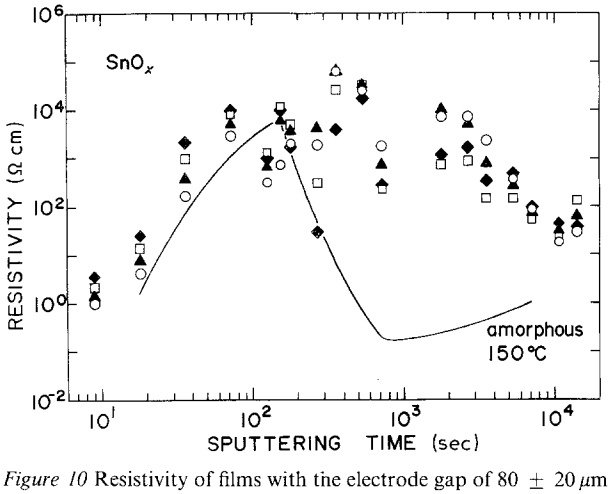

Figure 10 Resistivity of films with the electrode gap of 80 ± 20 μm in s-air. d = 80 μm. (○) 350° C, (▲) 300° C, (□) 250° C, (◆) 150° C.

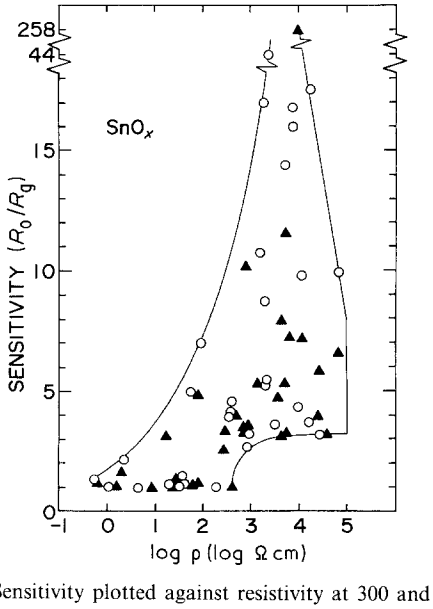

Figure 12 Sensitivity plotted against resistivity at 300 and 350° C. (○) 350° C, (▲) 300° C.

layer predominates and no boundary effect occurs. Certainly sensitivity and resistivity increased monotonically as the thickness decreased from 50 nm (1000 sec) to about 7 nm (140 sec) and both exhibited a maximum at about 7 nm [7]. For the thickest films, the reason why resistivity increased with thickness in crystalline as well as amorphous state as typically shown in Fig. 11, is not known. Because a given film is characterized by its resistivity in s-air as well as by its thickness, a plot of sensitivity as a function of resistivity is also interesting. Fig. 12 shows the plot at temperatures where thickness and grain boundary are expected to play an important role in determining the sensitivity. It is seen that highly sensitive films do not necessarily have the highest resistivity in s-air. The ten most sensitive films belong to a narrow thickness range from 60 to 180 nm, except one film 17 nm thick. It is also observed that the sensitivity minimum increases with resistivity for films with a resistivity higher than about 1000 Ωcm.

Hitherto we have often pointed out the importance of grain size. Grain growth depends not only on the heat treatment but also on the substrate material. Thus the effect of substrate on the sensor property was examined next.

3.5. Influence of substrate

The effects of five substrates with different thermal expansion coefficients were compared. Figs 13, 14 and 15 show the sensitivity and resistivity of films on these substrates as a function of thermal expansion coefficient. Films, 17 nm thick, on mullite, alumina and magnesia substrates have a high sensitivity at 350° C (Fig. 13) and their resistivities are comparable to, or smaller than, those on glass substrates (Fig. 14). On the other hand, the sensitivity of 87 nm thick films increases with increasing resistivity as shown in Fig. 15. Apparently we observe no unique relation between the sensor properties and the thermal expansion coefficients of substrates. The same was true for amorphous SnO_x films [7]. However, if we compare the properties of films on fused silica glass with those on pyrex glass (both substrates are fully dense and optically flat), we observe a difference. Because the thermal expansion coefficient of crystalline SnO_2 is

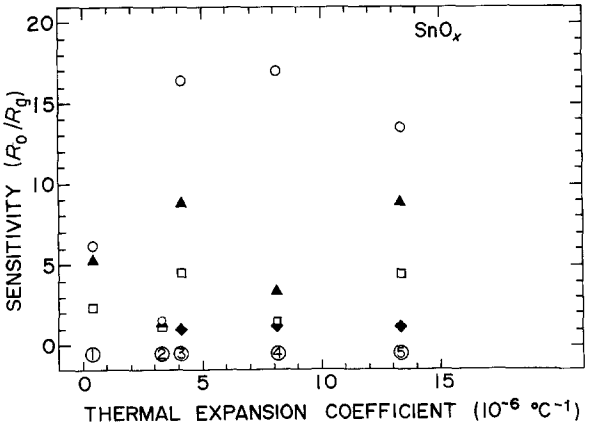

Figure 13 Sensitivity of films deposited on substrates with different thermal expansion coefficients. Thickness 17 nm, d = 455 μm. (○) 350° C, (▲) 300° C, (□) 250° C, (◆) 150° C, ①fused silica, ②pyrex, ③mullite, ④alumina, ⑤magnesia.

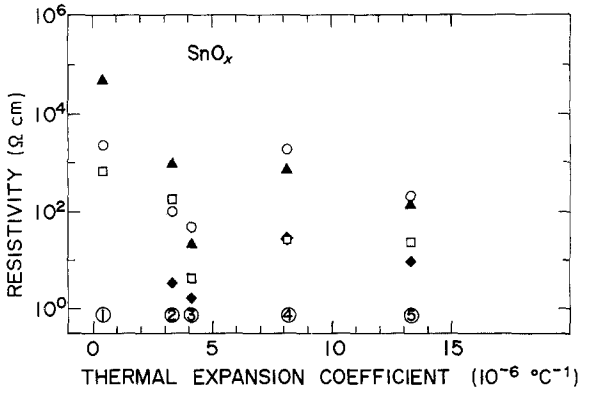

Figure 14 Resistivity of films deposited on substrates with different thermal expansion coefficients. Thickness 17 nm, d = 455 μm. (○) 350° C, (▲) 300° C, (□) 250° C, (◆) 150° C, ①fused silica, ②pyrex, ③mullite, ④alumina, ⑤magnesia.

reported to be 5×10^{-6} °C^{-1} [11], a large difference in expansion coefficient tends to increase the resistivity and sensitivity. This tendency seems to be contrary to the observation of De Waal and Simonis [12] that the induced intrinsic stresses within the SnO_2 coating increase the electrical conductivity.

These observations point out the importance of not only the thermal expansion coefficient and the film thickness, but also the surface roughness and the porosity of ceramic substrates.

4. Conclusion

1. 1 to 700 nm thick films were deposited on sintered alumina substrates by ion-beam sputtering.
2. Films annealed at 500° C for 2 h in air were mostly tetragonal SnO_2 with grains randomly oriented.
3. The film thickness exhibiting the sensitivity maximum gradually increased with temperature; it changed from 7 nm at 150° C to 175 nm at 350° C.
4. Highly sensitive films at 300 and 350° C mostly belonged to a narrow thickness range of 60 to 180 nm.
5. Sensor properties were influenced not only by the film thickness but also by the substrate material.
6. A model was proposed to interpret the influence of thickness on the sensitivity, in terms of grain boundary and depletion region.

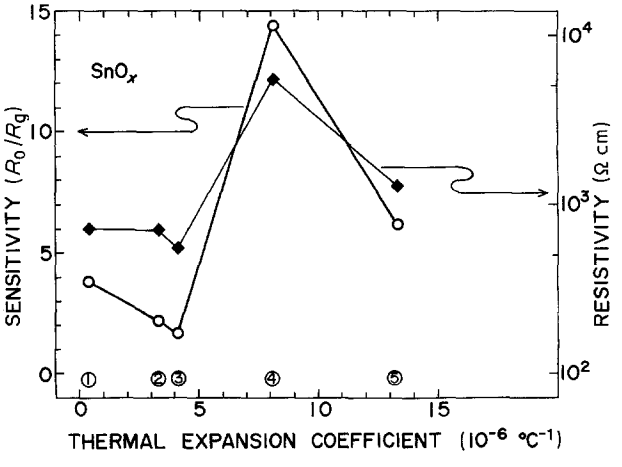

Figure 15 Sensitivity and resistivity of films deposited on substrates with different thermal expansion coefficients. Thickness 87 nm, d = 455 μm. ① Fused silica, ② pyrex, ③ mullite, ④ alumina, ⑤ magnesia, 350° C.

Acknowledgement

We would like to thank Professor N. Oyama of the Department of Applied Chemistry for Resources for help in film thickness analysis.

References

1. J. L. VOSSEN and E. S. POLINIAK, *Thin Solid Films* **13** (1972) 281.
2. U. DIBBERN, G. KÜRSTEN and P. WILLICH, in Proceedings of the 2nd International Meeting on Chemical Sensors, Bordeau, July 1986, edited by J. L. Aucouturier, L. S. Cauhape, M. Destriau, P. Hagenmuller, C. Lucat, F. Ménil, J. Portier and J. Salardenne (University of Bordeau, 1986) p. 127.
3. A. GRISEL and V. DEMARNE, *ibid.*, p. 247.
4. H. PINK, L. TREITINGER and L. VITÉ, *Jpn J. Appl. Phys.* **19** (1980) 513.
5. H. KANEKO and K. MIYAKE, *J. Appl. Phys.* **53** (1982) 3629.
6. D. BÉLANGER, J. P. DODELET, B. A. LOMBOS and J. I. DICKSON, *J. Electrochem. Soc.* **132** (1985) 1398.
7. T. SUZUKI, T. YAMAZAKI, H. YOSHIOKA and K. HIKICHI, *J. Mater. Sci.*, to be published.
8. T. SUZUKI and T. YAMAZAKI, *J. Mater. Sci. Lett.* **6** (1987) 1086.
9. T. SUZUKI, T. YAMAZAKI, H. YOSHIOKA, K. TAKAHASHI and T. KAGEYAMA, *J. Mater. Sci. Lett.* **6** (1987) 437.
10. N. YAMAZOE, J. FUCHIGAMI, M. KISHIKAWA and T. SEIYAMA, *Surface Sci.* **86** (1979) 335.
11. H. SEKI, N. ISHIZAWA, N. MIZUTANI and M. KATO, *Yogyo Kyokaishi* **92** (1984) 219.
12. H. DE WAAL and F. SIMONIS, *Thin Solid Films* **77** (1981) 253.

Received 8 June
and accepted 20 August 1987